RORγt^{+} innate lymphoid cells promote lymph node metastasis of breast cancers.

Sheeba Irshad[1]*, Fabian Flores-Borja[1,2]*, Katherine Lawler[2,3], James Monypenny[2], Rachel Evans[2], Victoria Male[1], Peter Gordon[1,2], Anthony Cheung[2], Patrycja Gazinska[1], Farzana Noor[1], Felix Wong[2], Anita Grigoriadis[1], Gilbert O Fruhwirth[2, 10], Paul R Barber[4], Natalie Woodman[5], Dominic Patel[11], Manuel Rodriguez-Justo[11], Julie Owen[5], Stewart Martin[6], Sarah E Pinder[5,7], Cheryl E. Gillett[5,7], Simon P Poland[2], Simon Ameer-Beg[2], Frank McCaughan[8,9], Leo M. Carlin[10], Uzma Hasan[11], David R Withers[12], Peter Lane[12], Borivoj Vojnovic[4], Sergio A Quezada[13], Paul Ellis[14], Andrew Tutt[1, 15] and Tony Ng[1,2,13].

[1]Breast Cancer Now Research Unit, KCL, London, SE1 9RT.

[2]Richard Dimbleby Department of Cancer Research, Randall Division & Division of Cancer Studies, KCL, Guy's Medical School Campus, SE1 1ULK.

[3] Institute for Mathematical and Molecular Biomedicine, KCL, Hodgkin Building, Guy's Medical School Campus, SE1 1UL.

[4]Gray Institute for Radiation Oncology & Biology, University of Oxford, Old Road Campus Research Building, Roosevelt Drive, Oxford OX3 7DQ.

[5]King's Health Partners Cancer Biobank, KCL, Guy's Hospital, London SE1 9RT.

[6]School of Medicine, Division of Cancer and Stem Cells, Department of Clinical Oncology, Nottingham University Hospitals NHS Trust, City Hospital Campus, Nottingham NG5 1PB

[7]Research Oncology, Division of Cancer Studies, KCL, 3rd Floor, Bermondsey Wing, Guy's Hospital, Great Maze Pond, London, SE1 9RT.

[8] Department of Asthma, Allergy, and Lung Biology, KCL, Guy's Hospital, Great Maze Pond, London, SE1 9RT.

[9]Department of Biochemistry, University of Cambridge, Cambridge

[10] Leukocyte Dynamics Group, Beatson Advanced Imaging Resource, CRUK Beatson Institute, Glasgow.

[11]International Center for Infectiology Research, University of Lyon, Lyon 69007, France; Inserm, U1111, Lyon 69007, France; Ecole Normale Supérieure de Lyon, Lyon 69007, France; Université Claude Bernard Lyon 1, Centre International de Recherche en Infectiologie, Lyon 69100, France; Centre National de la Recherche Scientifique, Unité Mixte de Recherche 5308, Lyon 69007, France; Oncovirus et l'immunité innée, Hospices Civils de Lyon Sud, Pierre Benite, 69495 France; uzma.hasan@inserm.fr.

[12]MRC Centre for Immune Regulation, Institute for Biomedical Research, College of Medical and Dental Sciences, University of Birmingham, Birmingham, B15 2TT.

[13] UCL Cancer Institute, Paul O'Gorman Building, University College London, London WC1E 6DD, UK

[14] Department of Medical Oncology, Guy's and St Thomas Foundation Trust, London SE1 9RT

[15] ICR, Breast Cancer Now Research Unit, Toby Robins Research Centre, London

Acknowledgement

Financial Support: KCL BCN Unit funding (J.Monypenny, F.Flores-Borja, A.Grigoriadis, V.Male), Sarah Greene Fellowship (S. Irshad), Dimbleby Cancer Care to KCL (Ameer-Beg and T.Ng), KCL-UCL CCIC funding (CR-UK & EPSRC, in association with the MRC and DoH England to T Ng) (R. Evans, N Woodman, S. Poland, K. Lawler, G Fruhwirth), CRUK programme grant (P. Barber and B. Vojnovic).

Supplemental Inventory

1. Supplemental Figures, Tables and Videos

Supplemental Figure S1, Related to Figure 1

Supplemental Figure S2, Related to Figure 2

Supplemental Figure S3, Related to Figure 2

Supplemental Figure S4, Related to Figure 4

Supplemental Figure S5, Related to Figure 5

Supplemental Figure S6, Related to Figure 5

Table S1, Related to Figure 5

Video S1, Related to Figure 2

Video S2, Related to Figure 2

2. Supplemental Experimental Procedures

Table S2: List of antibodies used

Table S3: Sequence of oligonucleotides used

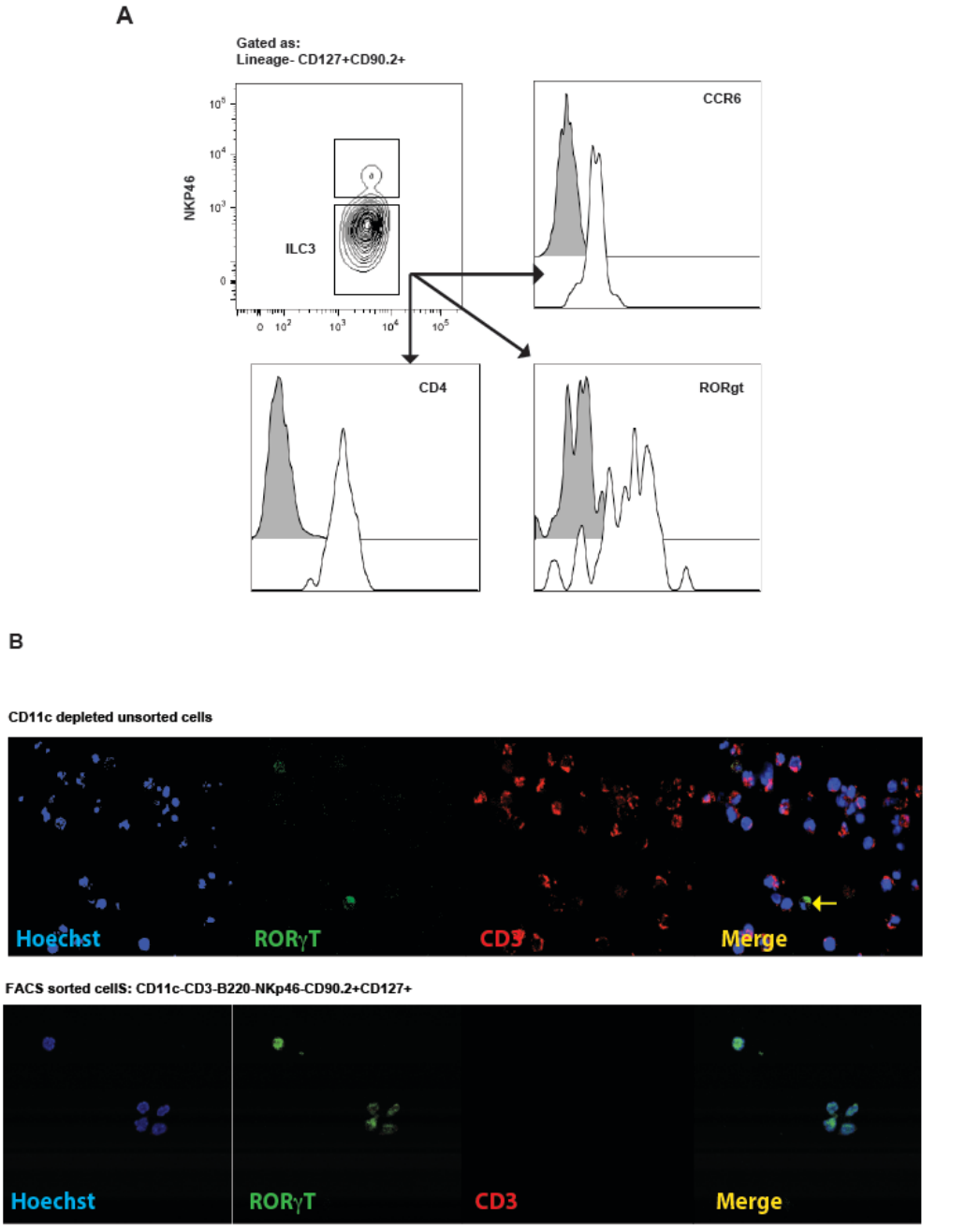

Figure S1, Related to Figure 1

A) FACS sorted $Lin^{-}CD127^{+}CD90.2^{+}NKP46^{-}$ gated cells in the primary tumor express additional markers CCR6, CD4 and RORγT that define LTi/ILC3. **B**) Immunofluorescence of unsorted CD11c-depleted splenocytes. An ILC3 cell (white arrow) is seen amongst $CD3^{+}$ cells. Bottom panel demonstrated that majority of the sorted cells express the nuclear transcription factor RORγT.

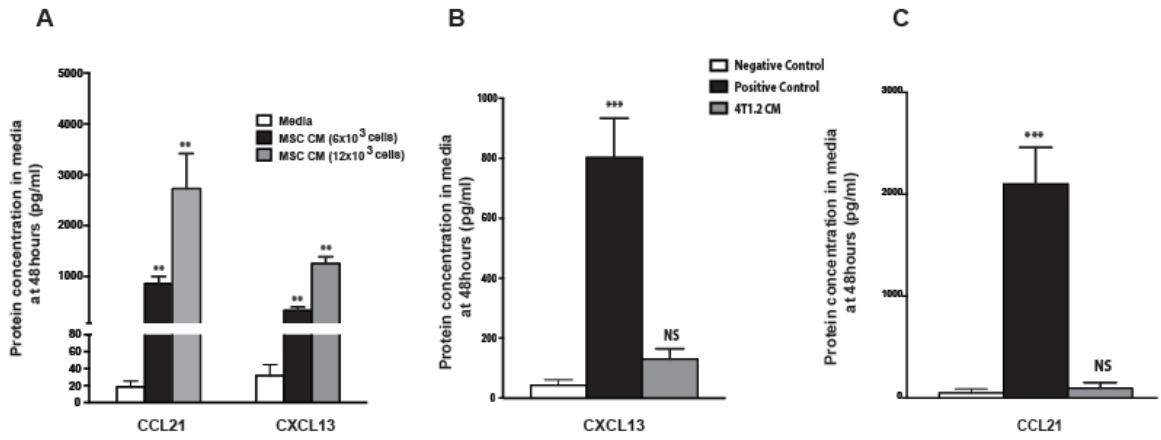

Figure S2, Related to Figure 2

A: Protein levels of CXCL13 and CCL21 in conditioned media (CM) obtained from the bone marrow derived MSC cell line (HS-5) compared to non-conditioned media were measured by ELISA. MSC cells seeded at densities of either $6x10^3$ or $12x10^3$ cells per well are shown above. Data represent means of three independent experiments ± SEM. **B & C:** ELISA quantification of CXCL13 and CCL21 chemokine levels in the conditioned media from the breast cancer cell line 4T1.2 cell line is shown. Positive control = murine stromal cell line (ST2s); Negative control = media alone. Asterisks represent the p-values when comparing to the control groups (one-way ANOVA; ** $p \leq 0.01$).

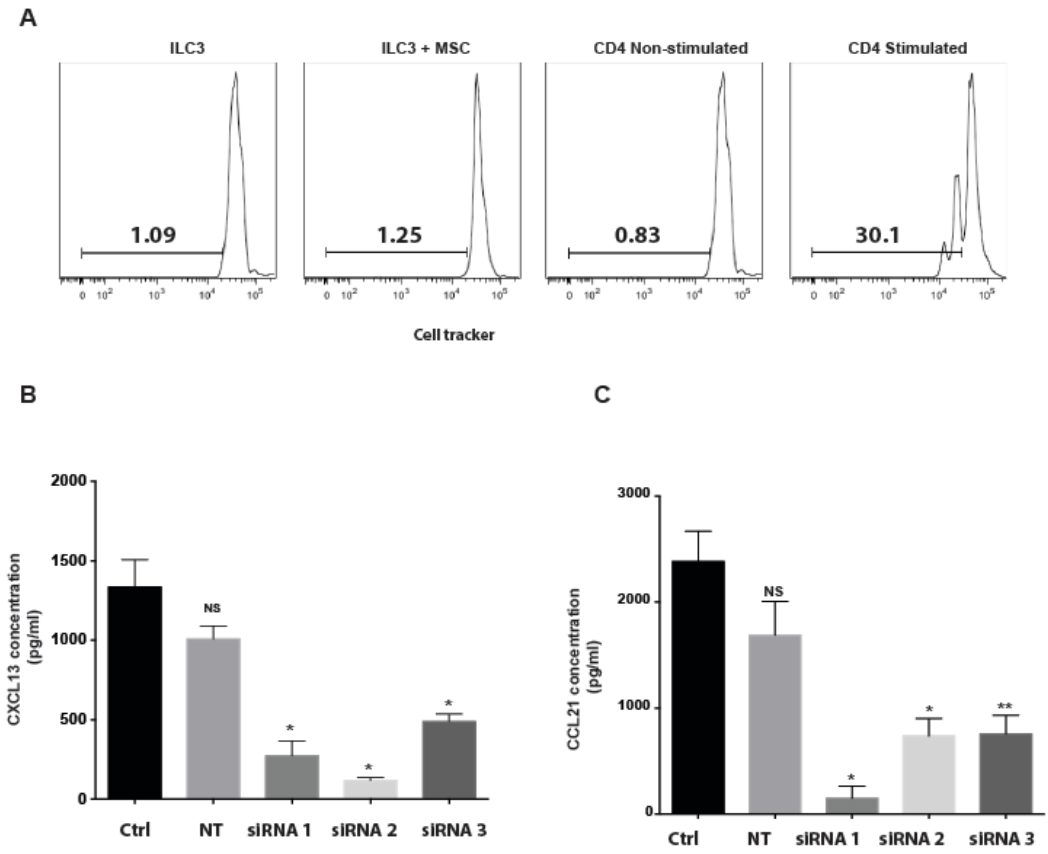

Figure S3, Related to Figure 2

A: ILC3 cells do not proliferate when co-cultured with human MSCs. FACS-sorted ILC3 cells were labelled with an eFluor450 cell tracker dye and co-cultured with human HS-5 MSC cell line (ratio 10:1, ILC3:MSC) for 48h. As proliferation positive control, cell-tracker dye-labelled splenocytes were stimulated with plate-bound anti-CD3 (1 μg/ml) and soluble anti-CD28 (2 μg/ml) antibodies. At the end of the co-culture cells were stained with a viability dye and analysed by flow cytometry. **B and C:** MSC cells were transfected with non targeting (NT) control or siRNAs specific for CXCL13 or CCL21 (CXCL13 siRNA: si-20725, si-20726, si-20727 or CCL21 siRNA: si-12605, si-12606, si-12607 etc respectively). Cell culture supernatents were analyzed by ELISA at 48hours (* $p \leq 0.05$, ** $p \leq 0.01$, paired t-test).

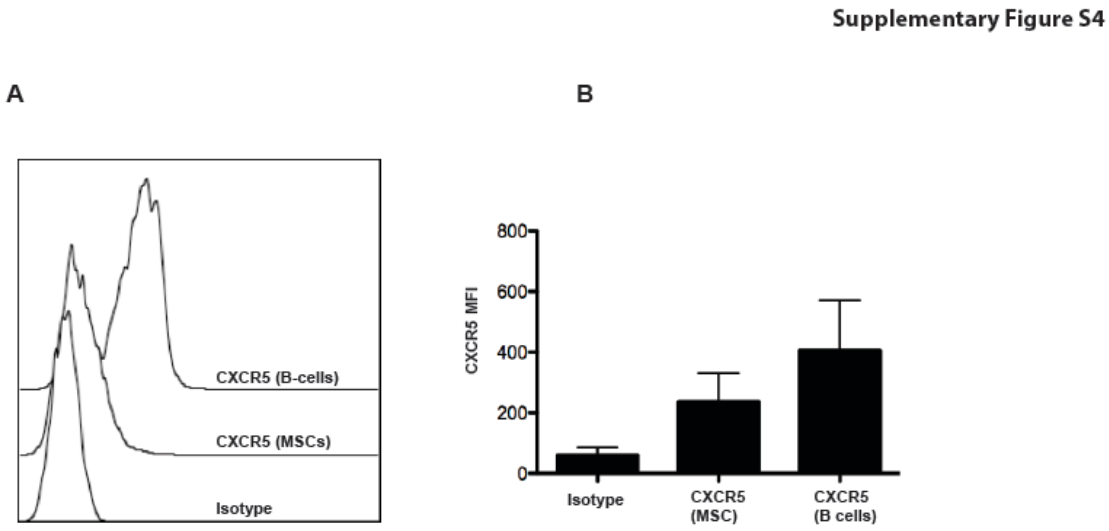

Figure S4, Related to Figure 4

A: CXCR5 expression on MSC cells. The histograms show the expression of CXCR5 on HS-5 human MSC cell line and human peripheral blood B-cells (positive control) as compared to control isotype antibody. The graph on the left shows cumulative data from three different experiments.

Supplementary Figure 5

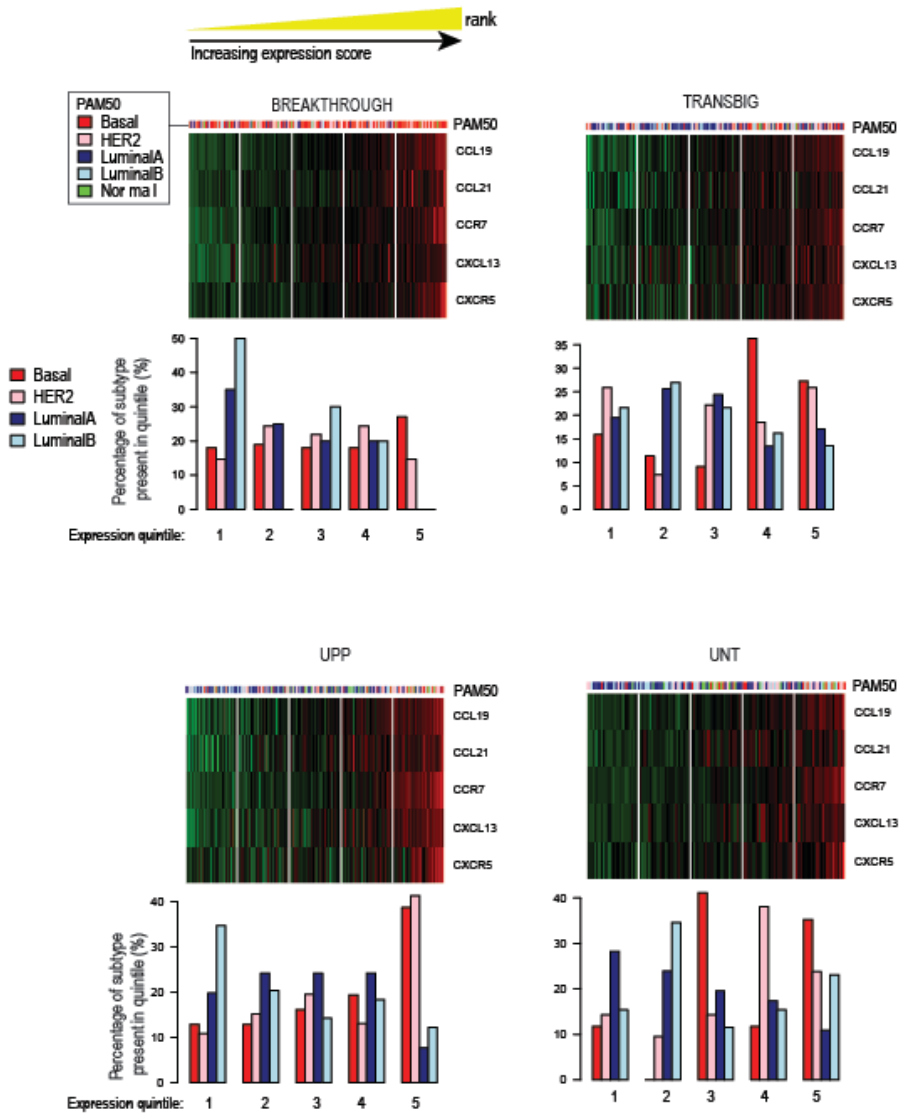

Figure S5, Related to Figure 5

Expression of lymphoid chemokine and chemokine receptor genes in breast cancer datasets. Heat maps display gene-standardised expression for each breast cancer data set. Columns (samples) are ordered by increasing expression score (mean of gene standardised expression values of the listed genes) and displayed in blocks representing score quintiles (left-right, lowest to highest expression score). PAM50 assignments are depicted above. Bar plots show the distribution of intrinsic subtype assignments within each expression quintile. Relative enrichment for the basal-like subtype (red) amongst samples with higher expression scores is observed in multiple independent data sets.

Supplementary Figure 6

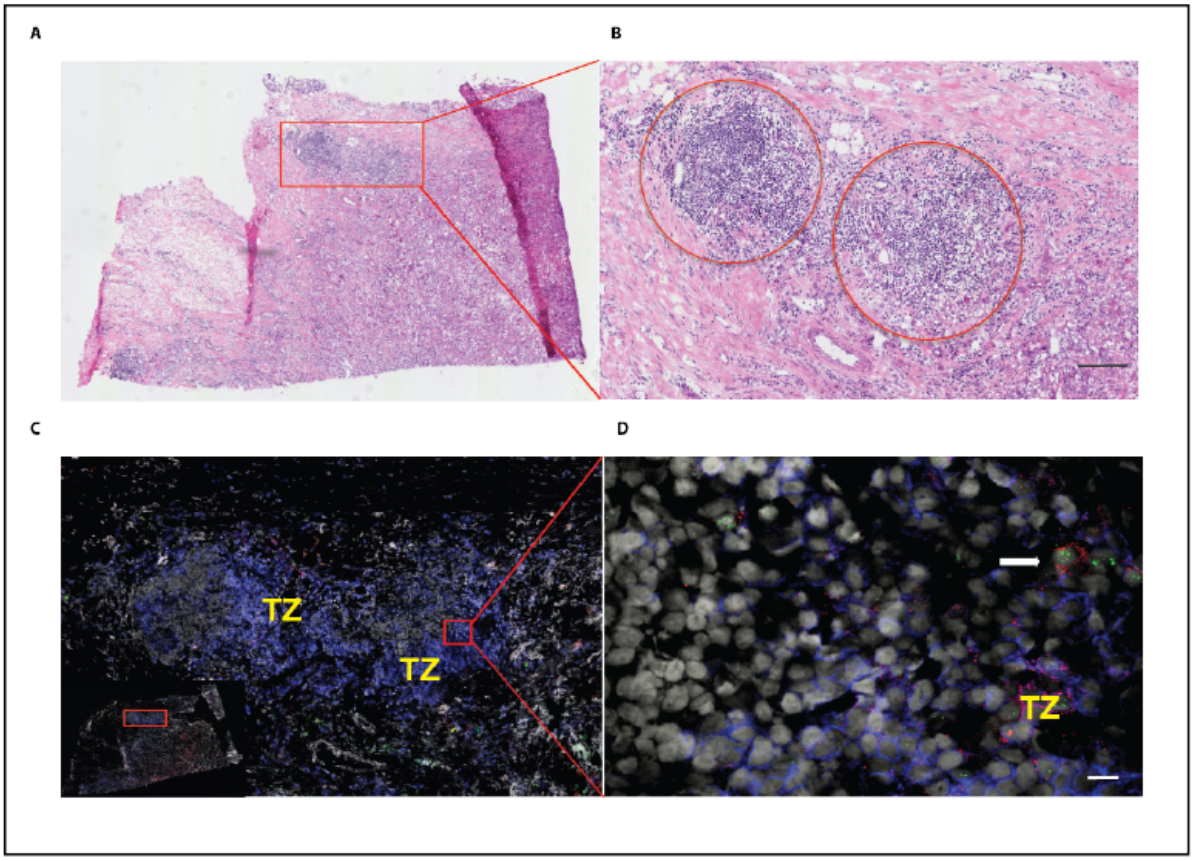

Figure S6, Related to Figure 5

Breast cancer tissue with prominent tertiary lymphoid follicle formation. Tumor infiltrating lymphocytes are not only scattered throughout the stroma and interspersed between tumor cells; they also cluster in aggregates resembling tertiary lymphoid tissue with distinct compartmentalization between a T and a B cell zone. **A:** H&E histopathological images show (**A**): Low power view of a breast cancer tumour section and (**B**): High power view allows identification of dense areas of lymphoid cell aggregates within the human breast cancer microenvironment (red circles). **C**: Immunofluorescence for CD3 (membrane or cytoplasmic blue staining) identifies the outer T-zone of these lymphoid structures. **D**: Identification of a RORγT+CD127+CD3- ILC3 cells (white arrow) (RORγT+, green nuclear; CD127+, red perinuclear) within the TLS. TZ=T zone. Red squares represent areas of interest.

Video S1, Related to Figure 2

Time lapse microscopy experiment of sorted NKp46$^-$ILC3 cells (CD3$^-$, CD11c$^-$, B220, NKp46$^-$, CD127$^+$, CD90.2$^+$) co-cultured with MSC cells as described in Figure 2B. Low magnification (×10) video shows the general clustering pattern of NKp46$^-$ILC3 cells around the MSC cells over a duration of 10 hours. Experimental conditions were as described in Figure 2B legend and in more detail in Experimental Procedures.

Video S2, Related to Figure 2

Time lapse microscopy experiment of sorted NKp46$^-$ILC3 cells (CD3$^-$, CD11c$^-$, B220$^-$, NKp46$^-$, CD127$^+$, CD90.2$^+$) co-cultured with MSC cells as described in Figure 2B. High magnification (×40) video shows the prolonged interaction of NKp46$^-$ILC3 and MSC cells upon contact. Experimental conditions were as described in Figure 2B legend and in more detailed in Experimental Procedures.

Supplementary Methods

Immunohistochemistry, Immunofluorescence and Image analysis

Immunohistochemistry of formalin-fixed, paraffin-embedded sections for podoplanin was performed on the Leica BOND-Max automated IHC platform (Leica Microsystems Inc, Wetzlar, Germany). Sections were incubated with monoclonal podoplanin antibody (18H5, diluted 1:1500 from Abcam, Cambridge, UK), and antigen binding detected using the Leica BOND refine polymer detection kit, DS9800. For immunohistochemistry of pan-cytokeratin, frozen sections were fixed in acetone and incubated with HRP-conjugated monoclonal pan-cytokeratin antibody (C11, diluted 1:500 from Santa Cruz Biotechnology, Santa Cruz, USA). Antigen binding was detected using ImmPACT DAB peroxidase substrate (Vector Labs, Burlingame, USA). Stained sections were photographed using a Hamamatsu NanoZoomer-XR C12000 digital slide scanner (Hamamatsu Photonics; Japan) and staining

areas were quantified using its integrated software.

For immunostaining of RANKL, cells were fixed (4% paraformaldehyde, 10 min), permeabilized (0.25% TritonX-100, 12 min at RT), blocked (1% BSA, 30 min) and incubated with the primary antibodies diluted in blocking solutions (see Table S2), followed by several washes with PBS and incubation with an suitable fluorescently conjugated secondary antibodies.

Time-lapse microscopy and image analysis

To measure the NKp46$^-$ILC3 clustering around stromal cells, series of image processing functions in ImageJ were performed to measure the area of the frame occupied by the cells. AVI videos were recorded in an RGB format and then converted to 8-bit grey-scale. Each frame of the video was treated independently and a 2-D rolling ball algorithm (aka grey-scale morphology) was run using the "Subtract Background" function with a ball radius of 10 pixels to remove interfering background variations. The Otsu algorithm ("Auto Threshold", "method = Otsu white"), was used to segment the foreground cells from the background by thresholding. On the resulting binary image the "Measure" function reports the average image intensity. This value divided by 255 equals the area proportion of foreground in the frame, for a binary image, and this was used to quantify the clustering. This algorithm has been implemented as an ImageJ macro running in batch mode, with a processing time of about 7 min for one 300-frame video. The macro is available from (http://users.ox.ac.uk/~atdgroup/software/ForegroundArea_batch.ijm**).**

ELISA

Tumors were snap frozen and lysed by homogenisation in 100mM Tris pH 7.5, 150mM NaCl, 1mM EGTA, 1mM EDTA, 1% (v/v) Triton-X-100 and 0.5% (w/v) sodium deoxycholate. ELISAs were performed using commercially available DuoSet kits (R&D Systems, Minneapolis, USA).

Supplementary Table S1: List of antibodies used

Name	Clone	Dilution	Company	Cross-reactivity to MS	Cross-reactivity to Hu
Rat anti-human RORγt	AFKJ5-9	1:25	Ebioscience	Yes	Yes
Mouse anti-human CD127 Biotin	ebioRDR5	1:25	Ebioscience	No	Yes
Mouse anti-human CD3 APC	UCHT1	1:30	Ebioscience	No	Yes
Dnk anti-Rat-IgG-FITC	-	1: 100	Jackson ImmunoResearch	Minimal	Minimal
Rabbit anti-rat IgG-FITC	-	1:200	Invitrogen	No	No
Goat anti-Rabbit-FITC	-	1:100	Southern Biotech	No	No
Streptavidin Alexa 555	-	1:500	Invitrogen	No	No
Mouse Anti-human gp36/podoplanin	18H5	1:1500	Abcam	No	Yes
Armenian Hamster anti-mouse CD3e-PE	145-2C11	1:200	Ebioscience	Yes	No
Armenian Hamster anti-mouse CD11c-FITC	N418	1:100	Miltenyi Biotec	Yes	No
Rat anti-mouse B220/CD45R- Alexa Flour® 646	RA3-6B2	1:150	Biolegend®	Yes	No
Rat anti-mouse CD127 (IL-7Ra)-PerCP/Cy5.5	A7R34	1:50	Biolegend®	Yes	No
Rat anti-mouse CD90.2-APC/Cy7	30-H12	1:50	Biolegend®	Yes	No
Rat anti-mouse CD335 (NKp46) eFluor® 450	29A1.4	1:100	ebioscience	Yes	No
Rabbit anti-human/mouse RANK	-	1:1000	Cell Signaling	Yes	Yes
Goat anti-mouse RANKL	-	1:500	R&D	Yes	No
Goat anti-mouse Pancytokeratin	-	1:500	Santa Cruz	Yes	Yes

Supplementary Table S2: Sequence of siRNA oligonucleotides

Gene	SiRNA ID	Target Sequence (5' -> 3')
CXCL13	S20727	CAAGCUGAAUGGAUACAAA
CXCL13	S20726	UGAUGGAAGUAUUGAGAAA
CXCL13	S20725	AUCGAAUUCAAAUCUUGGU
CCL21	S12606	CCAUCCCAGUAUCCUGUU
CCL21	S12605	CAGCUACCGAAGCAGGAA
CCL21	S12607	GCTATCCTGTTCTTGCCCCG
Scrambled	#10300934	Non-targeting siRNA pool from Thermo Scientific Dharmacon

Supplementary Table (S3):

Clinico-pathological characteristics for the METABRIC samples

Guy's METABRIC				
	(i) Gene expression data set		**(ii) Gene expression & ILC3 assay data set**	
	n = 234		*n = 59*	
	Number	(%)	Number	(%)
Age				
Median (y)	60.8		59.3	
Grade				
1	29	(12%)	3	(5%)
2	84	(36%)	12	(20%)
3	112	(48%)	42	(71%)
Unknown	9	(4%)	2	(3%)
ER (*ESR1* expression)				
Positive	176	(75%)	32	(54%)
Negative	58	(25%)	27	(46%)
Lymph nodes, no. positive				
0	95	(41%)	15	(25%)
1-3	93	(40%)	27	(46%)
4+	45	(19%)	17	(29%)
Unknown	1	(0.4%)	-	-
Invasive tumor size				
<= 2cm	100	(43%)	21	(36%)
> 2cm	134	(57%)	38	(64%)
Hormone treatment				
Yes	188	(80%)	39	(66%)
No	12	(5%)	4	(7%)
Unknown	34	(15%)	16	(27%)
Chemotherapy				
Yes	49	(21%)	28	(47%)
No	184	(79%)	31	(53%)
Unknown	1	(0.4%)	-	-

Table S1, Related to Figure 5

Table S1: Clinico-pathological characteristics for the METABRIC sample.

(i) Guy's METABRIC gene expression data set. Poor quality arrays were filtered out, leaving 234 out of a possible 250 samples for analysis for lymphoid gene expression analysis.

(ii) Guy's METABRIC gene expression data set stained for ILC3 density data (n=59).